Rotational structures in ^{155}Eu and ^{157}Tb

D. J. Hartley, M. A. Riley, D. E. Archer,* T. B. Brown, J. Döring,† R. A. Kaye, F. G. Kondev, T. Petters, J. Pfohl, R. K. Sheline, and S. L. Tabor
Department of Physics, Florida State University, Tallahassee, Florida 32306

J. Simpson
CCLRC, Daresbury Laboratory, Daresbury, Warrington, WA4 4AD, United Kingdom

(Received 28 January 1998)

High-spin states of ^{157}Tb were populated via the reactions ^{154}Sm(^{7}Li,4n) at 35 MeV and ^{150}Nd(^{11}B,4n) at 55 MeV. Previously known bands have been extended and one new structure has been identified. The rotational alignment behavior of the bands and band crossing systematics have been analyzed. Experimental $B(M1)/B(E2)$ ratios for the strongly coupled bands have been extracted and compared with theoretical predictions. New results were also obtained for the $N=92$ isotone ^{155}Eu. The [411]3/2 and [413]5/2 pseudospin partner bands were observed in both nuclei. Experimental $B(E1)/B(E2)$ ratios have been determined in both ^{155}Eu and ^{157}Tb. However, the estimated large $B(E1)$ strengths can be explained without static octupole deformation. The [411]3/2 bands in ^{155}Eu and ^{157}Tb have been found identical up to spin $I=\frac{23}{2}$, which might be explained by changes in deformation. [S0556-2813(98)04506-3]

PACS number(s): 21.10.Re, 23.20.Lv, 23.20.Gq, 27.70.+q

I. INTRODUCTION

Much work has been done over the last two decades on the odd-Z, odd-$A\approx 160$ nuclei in the rare-earth region. This area has proven to be fascinating due to the variety of structures resulting from the active proton orbitals and the softness of the nuclei with respect to deformation. A large number of high-spin phenomena has been investigated, for example, signature splitting and signature inversion [1,2], shape changes due to γ deformation [3,4], the persistence of proton pairing correlations at high spin [5], and band termination [6]. However, these studies have been limited to nuclei with $Z\geqslant 67$ largely because only beams of mass $A\leqslant 11$ may be used to obtain a significant cross section for the lighter nuclei. The promethium ($Z=61$) [7–11] and europium ($Z=63$) [12–17] nuclei have attracted much attention recently due to the possibility of octupole correlations in these nuclei. Thus far no comprehensive study of the terbium ($Z=65$) nuclei with a modern escape-suppressed Ge detector array has been performed. Valuable systematic features of the $A\approx 160$ region can be examined once the $N=88$–92 Tb nuclei have been studied. The present paper focuses on the $N=92$ nuclei ^{157}Tb and ^{155}Eu, while the results from our experimental investigations on ^{153,155}Tb will be published separately [18]. Previous studies, which used light beams (e.g., n and α beams), may be found in Refs. [19,20] and Refs. [21,22] for ^{157}Tb and ^{155}Eu, respectively.

II. EXPERIMENTAL DETAILS AND RESULTS

Two experiments were performed at the Florida State University tandem-linac facility which populated high-spin states in ^{157}Tb. One experiment employed the ^{154}Sm(^{7}Li,4n) reaction at 35 MeV and used a single target foil of thickness ≈ 5 mg/cm^2 of enriched (over 95%) ^{154}Sm, which was thick enough to stop the recoiling nuclei. The deexciting γ rays were detected using eight (four at 90° and four at 145° with respect to the beam direction) escape-suppressed Ge detectors in the Pittsburgh-Florida State Universities γ-ray array [23]. Approximately 9×10^7 events were recorded when two or more of the suppressed Ge detectors were in prompt coincidence ($\leqslant 100$ ns). The primary focus of this experiment was to produce data with good statistics for the extension of the level scheme and the analysis of directional correlations of oriented states (DCO) and $B(M1)/B(E2)$ ratios.

The significant collection of γ rays associated with ^{155}Eu (≈ 20% of the total data) from this experiment was formed through the ''massive transfer'' [24] reaction ^{154}Sm(^{7}Li,$\alpha 2n$) in which a portion of the ^{7}Li beam broke up into α (^{4}He) and tritium (^{3}H) particles. One would then expect to see the complementary ^{154}Sm(^{7}Li,$t2n$) reaction products leading to ^{156}Gd. The yrast band in ^{156}Gd was indeed seen to $I^{\pi}=12^{+}$ and the $2^{+}\rightarrow 0^{+}$ transition had an intensity of ≈ 30% of the strongest transition in ^{157}Tb. Since no new information on ^{156}Gd [25] was obtained, there is no reason to report any further on this nucleus.

Another experiment producing high-spin states in ^{157}Tb was performed using the reaction ^{150}Nd(^{11}B,4n) at a beam energy of 55 MeV. The target was ≈ 2 mg/cm^2 in thickness with a ≈ 15 mg/cm^2 thick Pb backing in order to stop the recoiling nuclei and thus minimize Doppler broadening effects. Seven escape-suppressed Ge detectors (four at 90° and three at 145°) were used in the Pittsburgh-Florida State Universities γ ray array. A total of 12×10^7 coincidence events were collected. This experiment focused primarily on producing even higher spin states than the ^{7}Li reaction for ^{157}Tb while still having a significant cross section. For this reason the beam energy was chosen to populate roughly equal

*Present address: Lawrence Livermore National Laboratory, Livermore, California 94550.

†Present address: Department of Physics, University of Notre Dame, Notre Dame, Indiana 46556.

amounts ($\approx$40% of the reaction products each) of $4n$ (^{157}Tb) and $5n$ (^{156}Tb) evaporation residues.

The data from the two experiments were sorted into separate $4k\times4k$ γ-γ coincidence matrices. The γ-ray energies were calibrated using a ^{152}Eu source while the detector efficiencies were determined using both the singles data from a ^{152}Eu source and coincident data from the experimentally produced even-even nucleus ^{156}Gd. The program ESCL8R [26] was used to analyze the coincidence spectra as well as to fit the corresponding γ-ray energies and relative intensities. The results are displayed in Tables I (^{157}Tb) and II (^{155}Eu), which contain excitation energies of the levels, transition energies, relative intensities, DCO ratios, and spin and parity assignments.

The determination of the spin assignments for new states found in ^{155}Eu [21,22] and ^{157}Tb [19,20] was based on previous work and on the use of DCO measurements. Spin and parity assignments in Tables I and II have been put in parentheses if reliable DCO values were not attainable. The DCO ratios [29] were calculated from the data by the expression

$$R_{\mathrm{DCO}}=\frac{I_{\gamma_1}(\text{at } 145°;\ \text{in coincidence with } \gamma_2 \text{ at } 90°)}{I_{\gamma_1}(\text{at } 90°;\ \text{in coincidence with } \gamma_2 \text{ at } 145°)},$$

where γ_2 is a stretched $E2$ transition. For averaging purposes and greater statistics, spectra in coincidence with three successive $E2$ transitions were summed for γ_2 whenever possible. Stretched $E2$ transitions ($\Delta I=2$) have $R_{\mathrm{DCO}}\approx1.0$, while $\Delta I=1$ transitions have ratios near 0.5 if the transitions have a small mixing ratio.

A. Level scheme of ^{157}Tb

In the previously published level schemes of ^{157}Tb found in Refs. [19,20], four rotational bands based on the quasiproton excitations of the [411]3/2, [532]5/2, [413]5/2, and [523]7/2 Nilsson levels were seen up to $I^\pi=\frac{19}{2}^+$, $\frac{19}{2}^-$, $\frac{11}{2}^+$, and $\frac{11}{2}^-$, respectively, as well as the bandhead of the [404]7/2 orbital. The composite level scheme from the two experiments performed in this work is shown in Fig. 1 and contains over 100 new transitions. In addition to extending the [411]3/2, [532]5/2, and [413]5/2 bands to higher spin, we have reassigned the [523]7/2 band and found a new decoupled sequence. Plots of the excitation energy (minus a rigid-rotor energy) and the relative intensities of the bands versus spin have been provided in Figs. 2(a) and 2(b), respectively, for further discussion. At this point, we should note that the level scheme of ^{157}Tb we present in this paper is different from that found in the Table of Isotopes [27] and in the most recent compilation of $A=157$ nuclei from Nuclear Data Sheets [28]. These references contain preliminary results for ^{157}Tb which are superseded by this work.

1. The [411]3/2 band

The Fermi level of ^{157}Tb has been calculated to be near the [411]3/2 proton orbital, which can be deduced from Fig. 3 for the predicted quadrupole deformation $\beta_2=0.257$ [30]. The [411]3/2 band was experimentally found to be the ground-state band of ^{157}Tb [31,32] and remains yrast up to spin $I=\frac{47}{2}$ [see Fig. 2(a)]. The combination of the two experiments has extended this strongly coupled band through the $i_{13/2}$ neutron alignment (see Sec. III) and up to the tentative $I=(\frac{55}{2})$ state. The summed spectrum in coincidence with the 426.9 and 452.9 keV transitions is shown in Fig. 4(a). Figure 2(b) indicates this band is the most intensely populated as is expected with its being yrast for the majority of the observed spin region.

2. The [532]5/2 band

This negative-parity band was observed up to spin $I=(\frac{51}{2})$ as can be seen in Fig. 1. Figure 4(b) displays a summed spectrum from transitions in coincidence with the 438.7 and 488.7 keV transitions of the [532]5/2 band. The band lies

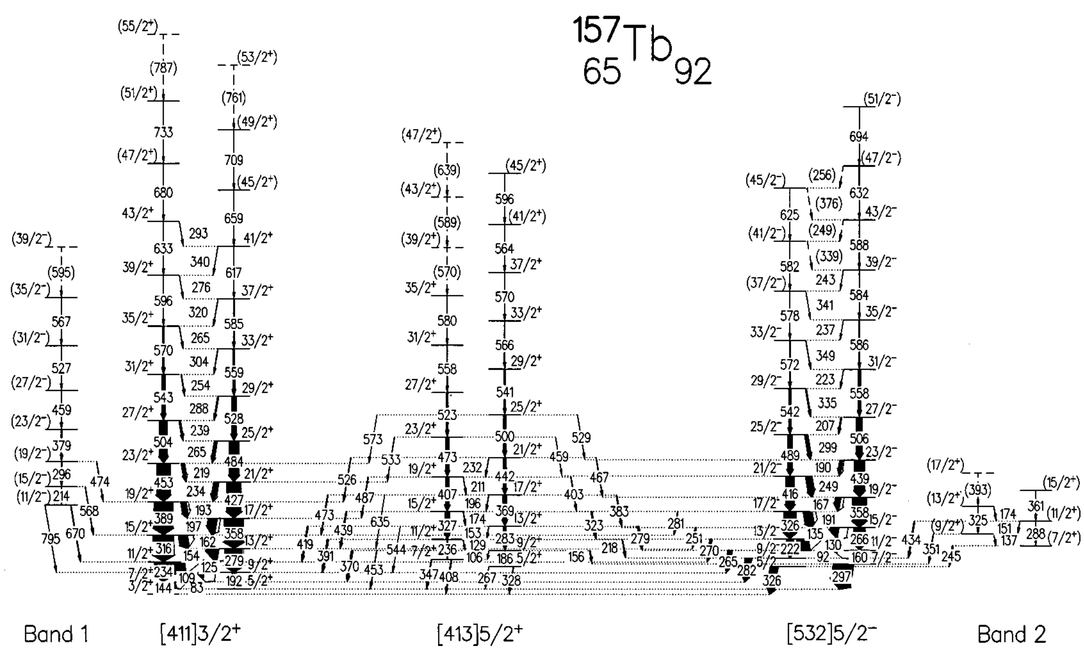

FIG. 1. Level scheme of ^{157}Tb. Tentative transitions and levels are denoted by dashed lines. Spin and parity assignments have been placed within parentheses if reliable DCO measurements were not attainable.

TABLE I. Results for ^{157}Tb.

E_x (keV) [a]	E_γ (keV) [b]	I_γ^{rel} [c]	I_γ^{rel} [d]	DCO ratio [e]	I_i^π [f]	I_f^π [f]
[411]3/2, $\alpha = +\frac{1}{2}$						
60.8	60.8 [g]				$\frac{5}{2}^+$	$\frac{3}{2}^+$
252.5	191.7	39(2)	43(2)	0.88(2) [h]	$\frac{9}{2}^+$	$\frac{5}{2}^+$
	108.8	90(5)	93(4)	0.88(3)	$\frac{9}{2}^+$	$\frac{7}{2}^+$
531.9	279.4	91(4)	82(4)	1.06(3)	$\frac{13}{2}^+$	$\frac{9}{2}^+$
	154.4	68(3)	60(3)	0.80(2)	$\frac{13}{2}^+$	$\frac{11}{2}^+$
890.2	358.3	95(4)	82(4)	1.01(2)	$\frac{17}{2}^+$	$\frac{13}{2}^+$
	196.8	47(2)	41(2)	0.75(2)	$\frac{17}{2}^+$	$\frac{15}{2}^+$
1317.1	426.9	72(3)	88(4)	0.99(3)	$\frac{21}{2}^+$	$\frac{17}{2}^+$
	234.1	23(1)	26(1)	0.76(4)	$\frac{21}{2}^+$	$\frac{19}{2}^+$
1800.8	483.7	48(2)	85(4)	0.94(2)	$\frac{25}{2}^+$	$\frac{21}{2}^+$
	264.9	13.0(6)	26(1)	0.69(2)	$\frac{25}{2}^+$	$\frac{23}{2}^+$
2328.3	527.5	23(1)	65(3)	0.99(3)	$\frac{29}{2}^+$	$\frac{25}{2}^+$
	288.2	5.7(3)	17.6(9)	0.63(3)	$\frac{29}{2}^+$	$\frac{27}{2}^+$
2887.2	558.9	9.3(5)	46(2)	1.05(5)	$\frac{33}{2}^+$	$\frac{29}{2}^+$
	304.3	2.3(1)	10.3(6)	0.76(8)	$\frac{33}{2}^+$	$\frac{31}{2}^+$
3472.5	585.3	4.4(2)	29(1)	0.95(6)	$\frac{37}{2}^+$	$\frac{33}{2}^+$
	319.9	1.4(1)	8.0(4)		$\frac{37}{2}^+$	$\frac{35}{2}^+$
4089.4	616.9	<1	17(1)	1.00(5) [j]	$\frac{41}{2}^+$	$\frac{37}{2}^+$
	340.3 [i]		4.4(3)		$\frac{41}{2}^+$	$\frac{39}{2}^+$
4748.0	658.6 [i]		7.2(5)		$(\frac{45}{2}^+)$	$\frac{41}{2}^+$
5456.5	708.5 [i]		1.1(3)		$(\frac{49}{2}^+)$	$(\frac{45}{2}^+)$
(6217.6)	(761.1 [i])		<1		$(\frac{53}{2}^+)$	$(\frac{49}{2}^+)$
[411]3/2, $\alpha = -\frac{1}{2}$						
143.8	143.8	≈ 10	≈ 15		$\frac{7}{2}^+$	$\frac{3}{2}^+$
	83.1	≈ 60			$\frac{7}{2}^+$	$\frac{5}{2}^+$
377.5	233.7	79(3)	85(6)	0.90(1) [h]	$\frac{11}{2}^+$	$\frac{7}{2}^+$
	125.1	78(3)	91(4)	0.83(2)	$\frac{11}{2}^+$	$\frac{9}{2}^+$
693.4	315.9	100	100	1.00(2)	$\frac{15}{2}^+$	$\frac{11}{2}^+$
	161.6	53(2)	55(3)	0.76(2)	$\frac{15}{2}^+$	$\frac{13}{2}^+$
1082.8	389.4	95(4)	105(5)	1.02(2)	$\frac{19}{2}^+$	$\frac{15}{2}^+$
	192.8	32(1)	35(2)	0.84(3) [h]	$\frac{19}{2}^+$	$\frac{17}{2}^+$
1535.7	452.9	68(3)	100(5)	0.95(2)	$\frac{23}{2}^+$	$\frac{19}{2}^+$
	218.6	14.5(7)	22(1)	0.71(2)	$\frac{23}{2}^+$	$\frac{21}{2}^+$
2040.1	504.4	41(2)	89(4)	0.97(2)	$\frac{27}{2}^+$	$\frac{23}{2}^+$
	239.2	7.2(3)	16.1(8)	0.60(3)	$\frac{27}{2}^+$	$\frac{25}{2}^+$
2582.7	542.6	16.9(8)	61(3)	0.96(3)	$\frac{31}{2}^+$	$\frac{27}{2}^+$
	254.4	2.9(2)	11.1(6)	0.72(4)	$\frac{31}{2}^+$	$\frac{29}{2}^+$
3152.6	569.9	8.3(4)	37(2)	0.98(5)	$\frac{35}{2}^+$	$\frac{31}{2}^+$
	265.3	1.5(1)	7.8(4)		$\frac{35}{2}^+$	$\frac{33}{2}^+$
3748.9	596.3	1.8(1)	27(2)	0.94(8) [j]	$\frac{39}{2}^+$	$\frac{35}{2}^+$
	276.3 [i]		4.6(4)		$\frac{39}{2}^+$	$\frac{37}{2}^+$
4381.8	632.9 [i]	<1	13.2(8)	0.9(1) [j]	$\frac{43}{2}^+$	$\frac{39}{2}^+$
	292.8 [i]		2.4(3)		$\frac{43}{2}^+$	$\frac{41}{2}^+$
5061.7	679.9 [i]		4.9(4)		$(\frac{47}{2}^+)$	$\frac{43}{2}^+$
5794.8	733.1 [i]		1.3(3)		$(\frac{51}{2}^+)$	$(\frac{47}{2}^+)$

TABLE I. (*Continued*).

E_x (keV) [a]	E_γ (keV) [b]	I_γ^{rel} [c]	I_γ^{rel} [d]	DCO ratio [e]	I_i^π [f]	I_f^π [f]
(6581.7)	(786.9 [i])		<1		$(\frac{55}{2}^+)$	$(\frac{51}{2}^+)$
[532]5/2, $\alpha = +\frac{1}{2}$						
326.4	326.4	≈40	≈30	0.66(4) [h]	$\frac{5}{2}^-$	$\frac{3}{2}^+$
425.6	99.1 [g]				$\frac{9}{2}^-$	$\frac{5}{2}^-$
	63.8 [g]				$\frac{9}{2}^-$	$\frac{7}{2}^-$
	281.8	33(1)	37(2)	0.56(2)	$\frac{9}{2}^-$	$\frac{7}{2}^+$
647.8	222.2	30(1)	28(1)	0.97(5)	$\frac{13}{2}^-$	$\frac{9}{2}^-$
	130.4	57(3)	61(3)	0.91(4)	$\frac{13}{2}^-$	$\frac{11}{2}^-$
	270.2	8.6(4)	10.3(7)	0.60(4)	$\frac{13}{2}^-$	$\frac{11}{2}^+$
974.2	326.4	54(3)	59(3)	0.92(2) [h]	$\frac{17}{2}^-$	$\frac{13}{2}^-$
	191.1	49(2)	47(2)	0.77(3) [h]	$\frac{17}{2}^-$	$\frac{15}{2}^-$
	280.8	4(1)			$\frac{17}{2}^-$	$\frac{15}{2}^+$
1390.2	416.0	44(2)	50(2)	1.02(4)	$\frac{21}{2}^-$	$\frac{17}{2}^-$
	249.0	28(1)	34(2)	0.71(3)	$\frac{21}{2}^-$	$\frac{19}{2}^-$
1878.9	488.7	25(1)	42(2)	0.95(4)	$\frac{25}{2}^-$	$\frac{21}{2}^-$
	298.8	14.6(7)	30(1)	0.60(1) [h]	$\frac{25}{2}^-$	$\frac{23}{2}^-$
2420.9	542.0	12.5(6)	37(2)	1.04(5)	$\frac{29}{2}^-$	$\frac{25}{2}^-$
	334.6	5.6(3)	18.2(9)	0.66(4)	$\frac{29}{2}^-$	$\frac{27}{2}^-$
2993.2	572.3	6.1(3)	29(1)	0.97(6) [j]	$\frac{33}{2}^-$	$\frac{29}{2}^-$
	349.2	2.4(2)	11.7(6)		$\frac{33}{2}^-$	$\frac{31}{2}^-$
3571.1	577.9	1.9(1)	18.2(9)	1.0(1) [j]	$(\frac{37}{2}^-)$	$\frac{33}{2}^-$
	340.9 [i]	<1	8.6(4)		$(\frac{37}{2}^-)$	$\frac{35}{2}^-$
4153.1	582.0 [i]		13.7(8)		$(\frac{41}{2}^-)$	$(\frac{37}{2}^-)$
	(339.3 [i])		4.4(4)		$(\frac{41}{2}^-)$	$\frac{39}{2}^-$
4778.1	625.0 [i]		5.2(4)		$(\frac{45}{2}^-)$	$(\frac{41}{2}^-)$
	(376.0 [i])		2.3(3)		$(\frac{45}{2}^-)$	$\frac{43}{2}^-$
[532]5/2, $\alpha = -\frac{1}{2}$						
357.6	296.8	≈190	≈170	0.63(3)	$\frac{7}{2}^-$	$\frac{5}{2}^+$
517.6	160.0	9.0(4)	8.1(4)	1.2(2)	$\frac{11}{2}^-$	$\frac{7}{2}^-$
	91.7	38(1)	38(2)		$\frac{11}{2}^-$	$\frac{9}{2}^-$
	265.0	24(1)	23(1)	0.85(2) [h]	$\frac{11}{2}^-$	$\frac{9}{2}^+$
783.2	265.6	54(2)	46(2)	0.85(2) [h]	$\frac{15}{2}^-$	$\frac{11}{2}^-$
	135.2	43(2)	48(2)	0.84(2)	$\frac{15}{2}^-$	$\frac{13}{2}^-$
	251.2	6.1(4)	7.5(6)	0.57(6)	$\frac{15}{2}^-$	$\frac{13}{2}^+$
1141.4	358.2	66(3)	84(4)	1.01(2)	$\frac{19}{2}^-$	$\frac{15}{2}^-$
	167.0	30(1)	39(2)	0.70(3)	$\frac{19}{2}^-$	$\frac{17}{2}^-$
1580.1	438.7	50(2)	79(4)	1.00(4)	$\frac{23}{2}^-$	$\frac{19}{2}^-$
	189.9	13.2(7)	24(1)	0.69(5) [h]	$\frac{23}{2}^-$	$\frac{21}{2}^-$
2086.3	506.2	29(1)	74(4)	0.95(4)	$\frac{27}{2}^-$	$\frac{23}{2}^-$
	207.2	6.0(2)	15.1(7)	0.61(4)	$\frac{27}{2}^-$	$\frac{25}{2}^-$
2644.1	557.8	13.2(6)	54(3)	1.02(4)	$\frac{31}{2}^-$	$\frac{27}{2}^-$
	223.1	2.1(1)	9.3(6)		$\frac{31}{2}^-$	$\frac{29}{2}^-$
3229.9	585.8	5.4(3)	34(2)	1.02(8) [h,j]	$\frac{35}{2}^-$	$\frac{31}{2}^-$
	236.7 [i]	<1	5.0(4)		$\frac{35}{2}^-$	$\frac{33}{2}^-$
3813.6	583.7 [i]	1.7(1)	25(1)	0.98(9) [j]	$\frac{39}{2}^-$	$\frac{35}{2}^-$

TABLE I. (*Continued*).

E_x (keV) [a]	E_γ (keV) [b]	$I_\gamma^{\rm rel}$ [c]	$I_\gamma^{\rm rel}$ [d]	DCO ratio [e]	I_i^π [f]	I_f^π [f]
	242.5 [i]	<1	3.9(3)		$\frac{39}{2}^-$	$(\frac{37}{2}^-)$
4401.9	588.3 [i]		10.6(6)	1.02(8) [h,j]	$\frac{43}{2}^-$	$\frac{39}{2}^-$
	(249.0 [i])		1.8(5)		$\frac{43}{2}^-$	$(\frac{41}{2}^-)$
5034.0	632.1 [i]		6.2(4)		$(\frac{47}{2}^-)$	$\frac{43}{2}^-$
	(255.8 [i])		<1		$(\frac{47}{2}^-)$	$(\frac{45}{2}^-)$
5728.0	694.0 [i]		3.6(3)		$(\frac{51}{2}^-)$	$(\frac{47}{2}^-)$
[413]5/2, $\alpha=+\frac{1}{2}$						
327.6	327.6	≈ 3		0.78(9) [h]	$\frac{5}{2}^+$	$\frac{3}{2}^+$
	266.6	1.3(1)		0.80(7) [h]	$\frac{5}{2}^+$	$\frac{5}{2}^+$
513.9	186.3	3.1(1)	1.0(2)		$\frac{9}{2}^+$	$\frac{5}{2}^+$
	105.7	<1			$\frac{9}{2}^+$	$\frac{7}{2}^+$
	370.0	10.5(7)	2.8(3)	0.81(4) [h]	$\frac{9}{2}^+$	$\frac{7}{2}^+$
	156.2	4.5(2)	1.3(3)		$\frac{9}{2}^+$	$\frac{7}{2}^-$
	453.3	2.8(2)			$\frac{9}{2}^+$	$\frac{5}{2}^+$
797.0	283.1	14.0(6)	5.5(4)		$\frac{13}{2}^+$	$\frac{9}{2}^+$
	153.3	1.1(1)			$\frac{13}{2}^+$	$\frac{11}{2}^+$
	419.4	6.5(3)	2.8(3)	0.46(3)	$\frac{13}{2}^+$	$\frac{11}{2}^+$
	279.4	9.8(5)	3.6(5)	0.67(3) [h]	$\frac{13}{2}^+$	$\frac{11}{2}^-$
	544.3	<1			$\frac{13}{2}^+$	$\frac{9}{2}^+$
1166.3	369.3	18.7(9)	8.6(6)	0.81(4) [h]	$\frac{17}{2}^+$	$\frac{13}{2}^+$
	195.9	1.5(1)			$\frac{17}{2}^+$	$\frac{15}{2}^+$
	472.8	4.6(3)	2.0(3)	0.58(5)	$\frac{17}{2}^+$	$\frac{15}{2}^+$
	383.3	5.5(3)	2.4(3)	0.58(7)	$\frac{17}{2}^+$	$\frac{15}{2}^-$
	634.7	<1			$\frac{17}{2}^+$	$\frac{13}{2}^+$
1608.6	442.3	16.3(7)	13.2(8)	0.98(4)	$\frac{21}{2}^+$	$\frac{17}{2}^+$
	231.8	<1			$\frac{21}{2}^+$	$\frac{19}{2}^+$
	525.5	3.8(2)	3.3(4)		$\frac{21}{2}^+$	$\frac{19}{2}^+$
	467.2	2.8(2)	2.0(3)		$\frac{21}{2}^+$	$\frac{19}{2}^-$
2108.7	500.1	12.6(6)	13.4(4)	1.04(6)	$\frac{25}{2}^+$	$\frac{21}{2}^+$
	572.5	2.8(2)	3.1(5)		$\frac{25}{2}^+$	$\frac{23}{2}^+$
	528.7	1.7(1)			$\frac{25}{2}^+$	$\frac{23}{2}^-$
2649.8	541.1	6.3(3)	12.7(7)	0.89(6)	$\frac{29}{2}^+$	$\frac{25}{2}^+$
3216.1	566.3	2.8(2)	11.6(6)	0.96(3)	$\frac{33}{2}^+$	$\frac{29}{2}^+$
3785.7	569.6 [i]	<1	8.6(6)	1.0(1) [j]	$\frac{37}{2}^+$	$\frac{33}{2}^+$
4349.8	564.1 [i]		5.9(4)		$(\frac{41}{2}^+)$	$\frac{37}{2}^+$
4945.7	595.9 [i]		4.1(4)		$(\frac{45}{2}^+)$	$(\frac{41}{2}^+)$
[413]5/2, $\alpha=-\frac{1}{2}$						
408.0	408.0	≈ 5		0.97(5) [h]	$\frac{7}{2}^+$	$\frac{3}{2}^+$
	347.1	3.9(3)			$\frac{7}{2}^+$	$\frac{5}{2}^+$
643.5	235.5	6.9(3)	2.3(3)	0.97(8)	$\frac{11}{2}^+$	$\frac{7}{2}^+$
	129.2	<1			$\frac{11}{2}^+$	$\frac{9}{2}^+$
	390.8	9.2(4)	2.5(4)	0.67(4)	$\frac{11}{2}^+$	$\frac{9}{2}^+$

TABLE I. (*Continued*).

E_x (keV) [a]	E_γ (keV) [b]	I_γ^{rel} [c]	I_γ^{rel} [d]	DCO ratio [e]	I_i^π [f]	I_f^π [f]
	217.7	6.1(3)	2.0(3)	0.76(6)	$\frac{11}{2}^+$	$\frac{9}{2}^-$
970.4	326.9	22.9(9)	7.8(7)	0.98(3)	$\frac{15}{2}^+$	$\frac{11}{2}^+$
	173.5	1.5(1)			$\frac{15}{2}^+$	$\frac{13}{2}^+$
	438.7	6.5(3)	2.4(3)	0.31(3)	$\frac{15}{2}^+$	$\frac{13}{2}^+$
	322.7	8.6(3)	2.8(3)	0.58(3)	$\frac{15}{2}^+$	$\frac{13}{2}^-$
1376.9	406.5	19.0(9)	10.7(7)	0.97(5) [h]	$\frac{19}{2}^+$	$\frac{15}{2}^+$
	211.0	1.0(1)			$\frac{19}{2}^+$	$\frac{17}{2}^+$
	486.9	3.2(2)	2.9(3)	0.45(7)	$\frac{19}{2}^+$	$\frac{17}{2}^+$
	402.6	4.1(2)	2.8(3)	0.63(6)	$\frac{19}{2}^+$	$\frac{17}{2}^-$
1849.4	472.5	16.2(7)	15(1)	0.99(5)	$\frac{23}{2}^+$	$\frac{19}{2}^+$
	532.5	2.0(1)			$\frac{23}{2}^+$	$\frac{21}{2}^+$
	459.0	1.6(1)			$\frac{23}{2}^+$	$\frac{21}{2}^-$
2372.6	523.2	8.2(4)	13.7(8)	0.93(6)	$\frac{27}{2}^+$	$\frac{23}{2}^+$
2930.9	558.3	3.2(2)	11.6(8)	1.02(4)	$\frac{31}{2}^+$	$\frac{27}{2}^+$
3511.0	580.1	1.1(1)	6.2(4)	1.1(1) [j]	$\frac{35}{2}^+$	$\frac{31}{2}^+$
(4080.5)	(569.5 [i])		3.3(3)		$(\frac{39}{2}^+)$	$\frac{35}{2}^+$
(4669.1)	(588.6 [i])		2.9(3)		$(\frac{43}{2}^+)$	$(\frac{39}{2}^+)$
(5307.6)	(638.5 [i])		2.4(3)		$(\frac{47}{2}^+)$	$(\frac{43}{2}^+)$
Band 1, $\alpha=-\frac{1}{2}$						
1047.1	669.6	2.9(3)			$(\frac{11}{2}^-)$	$\frac{11}{2}^+$
	795.2	<1			$(\frac{11}{2}^-)$	$\frac{9}{2}^+$
1261.0	213.9	2.1(2)	2.3(2)		$(\frac{15}{2}^-)$	$(\frac{11}{2}^-)$
	567.5	<1	1.1(2)		$(\frac{15}{2}^-)$	$\frac{15}{2}^+$
1556.6	295.6	4.2(2)	4.1(3)		$(\frac{19}{2}^-)$	$(\frac{15}{2}^-)$
	473.5	2.0(2)	1.3(2)		$(\frac{19}{2}^-)$	$\frac{19}{2}^+$
1935.1	378.5	3.9(2)	3.3(3)		$(\frac{23}{2}^-)$	$(\frac{19}{2}^-)$
2394.0	458.9	2.6(1)	3.1(3)		$(\frac{27}{2}^-)$	$(\frac{23}{2}^-)$
2920.8	526.8	1.1(1)	2.8(3)		$(\frac{31}{2}^-)$	$(\frac{27}{2}^-)$
3487.6	566.8	<1			$(\frac{35}{2}^-)$	$(\frac{31}{2}^-)$
(4082.3)	(594.7)	<1			$(\frac{39}{2}^-)$	$(\frac{35}{2}^-)$
Band 2, $\alpha=+\frac{1}{2}$						
708.8	137.3	<1			$(\frac{9}{2}^+)$	$(\frac{7}{2}^+)$
	351.2	<1			$(\frac{9}{2}^+)$	$\frac{7}{2}^-$
1033.9	325.1	<1			$(\frac{13}{2}^+)$	$(\frac{9}{2}^+)$
	173.9	<1			$(\frac{13}{2}^+)$	$(\frac{11}{2}^+)$
(1426.6)	(392.7)	<1			$(\frac{17}{2}^+)$	$(\frac{13}{2}^+)$
Band 2, $\alpha=-\frac{1}{2}$						
571.7	245.3	1.1(1)			$(\frac{7}{2}^+)$	$\frac{5}{2}^-$
859.4	287.7	<1			$(\frac{11}{2}^+)$	$(\frac{7}{2}^+)$
	151.2	<1			$(\frac{11}{2}^+)$	$(\frac{9}{2}^+)$

TABLE I. (*Continued*).

E_x (keV) [a]	E_γ (keV) [b]	I_γ^{rel} [c]	I_γ^{rel} [d]	DCO ratio [e]	I_i^π [f]	I_f^π [f]
	434.2	<1			$(\frac{11}{2}^+)$	$\frac{9}{2}^-$
1220.1	360.7	<1			$(\frac{15}{2}^+)$	$(\frac{11}{2}^+)$

[a]Bandhead excitation energies have been taken from previous work [19,20] except for band 1.
[b]Energies determined from the ^{154}Sm(^{7}Li,4n) reaction unless otherwise noted. Accurate to 0.2 keV for most transitions. For weak or contaminated transitions, accurate to 0.5 keV.
[c]Relative γ-ray intensities $[I_\gamma(315.9)\equiv 100]$ measured from the ^{154}Sm(^{7}Li,4n) reaction.
[d]Relative γ-ray intensities $[I_\gamma(315.9)\equiv 100]$ measured from the ^{150}Nd(^{11}B,4n) reaction.
[e]DCO ratios were determined by summing spectra in coincidence with one or more stretched $E2$ transitions as gates. Unless otherwise noted, DCO ratios were measured using the ^{154}Sm(^{7}Li,4n) reaction.
[f]Spin and parity assignments are based on the previous work [19,20] and on the DCO ratio determining the multipolarity of any new transition.
[g]Transition was not observed in this work, but was seen in previous publications [19,20].
[h]DCO value has been contaminated by an unresolvable doublet of different multipolarity.
[i]Energy determined from the ^{150}Nd(^{11}B,4n) reaction.
[j]DCO ratio determined from the ^{150}Nd(^{11}B,4n) reaction.

near the [411]3/2 band in excitation energy above $I=\frac{19}{2}$, and in fact the $\alpha=-\frac{1}{2}$ signature becomes yrast at $I=(\frac{47}{2})$, see Fig. 2(a). One may also notice the relatively large separation between the two signatures of this band in Figs. 1 and 2(a). The $\alpha=-\frac{1}{2}$ signature is energetically favored over the $\alpha=+\frac{1}{2}$ signature under nuclear rotation which causes the staggering effect in the intensity profile, Fig. 2(b), as well as other signature dependent behavior. The [532]5/2 band decays into the [411]3/2 band via a series of seven $E1$ transitions.

3. The [413]5/2 band

The [413]5/2 band has been extended from $I=\frac{11}{2}$ up to $I=(\frac{47}{2})$. A coincidence spectrum is provided in Fig. 4(c). Figure 2(a) shows that the signature partners have nearly the same excitation energies up to spin $I=(\frac{39}{2})$. This is reflected in the intensity profile of Fig. 2(b) where no signature effects are seen; however, one may observe the reduction in intensity below $I=\frac{15}{2}$, where the [413]5/2 strongly depopulates into the two previously discussed bands. The band feeds into the yrast [411]3/2 band through eleven $\Delta I=1$ transitions and three stretched $E2$ transitions. The [413]5/2 band also strongly feeds the [532]5/2 band through a series of nine $\Delta I=1$ $E1$ transitions. A discussion of the $B(E1)$ strengths for these as well as the other $E1$ transitions in ^{155}Eu and ^{157}Tb is presented in Sec. IV B.

4. Band 1

This weakly populated band ($\approx 3\%$ of the yrast band) is displayed in Fig. 4(d). The estimated spin assignments have largely been based on the intensity profile in Fig. 2(b). Since the low-spin states lie much higher in energy (≈ 400 keV above the [413]5/2 band at $I=(\frac{11}{2})$) compared with the other bands, this band was most likely populated at higher spin. This is supported by observing the virtually flat intensity profile displayed in Fig. 2(b). By assigning the lowest state of the band a spin value of $I=\frac{11}{2}$, it can be seen that at high-spin $[I=(\frac{31}{2})]$ the [413]5/2 band and band 1 have very similar excitation energy [Fig. 2(a)]. We therefore expect the intensities of these two bands to be nearly equal at $I\geqslant(\frac{31}{2})$ if this spin assignment is correct. Figure 2(b) indicates that our expectation is confirmed and that any other spin assignment contradicts the intensity profile. Unfortunately, due to the weakness of the band, DCO measurements were not possible on any of the connecting transitions to add validity to our

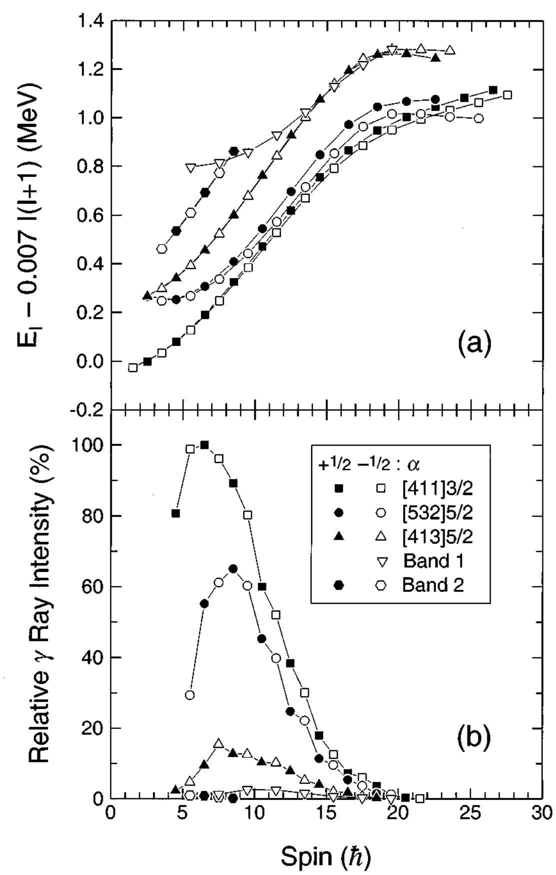

FIG. 2. (a) Excitation energy (minus a rigid-rotor energy) versus spin for ^{157}Tb. (b) Relative intensity of the bands in ^{157}Tb versus spin from the ^{7}Li experiment.

TABLE II. Results for ^{155}Eu.

E_x (keV) [a]	E_γ (keV) [b]	I_γ^{rel} [c]	DCO ratio [d]	I_i^π [e]	I_f^π [e]
[413]5/2, $\alpha=+\frac{1}{2}$					
179.2	179.2	100	0.77(4) [g]	$\frac{9}{2}^+$	$\frac{5}{2}^+$
	100.6	52(3)		$\frac{9}{2}^+$	$\frac{7}{2}^+$
443.0	263.8	63(3)	1.03(4)	$\frac{13}{2}^+$	$\frac{9}{2}^+$
	142.4	8.1(4)		$\frac{13}{2}^+$	$\frac{11}{2}^+$
	85.8	8.9(6)	0.7(1)	$\frac{13}{2}^+$	$\frac{11}{2}^-$
785.3	342.3	29(1)	1.04(7)	$\frac{17}{2}^+$	$\frac{13}{2}^+$
	181.0	2.6(2)		$\frac{17}{2}^+$	$\frac{15}{2}^+$
	160.8	6.3(4)	0.60(8) [g]	$\frac{17}{2}^+$	$\frac{15}{2}^-$
1198.2	412.9	13.1(7)	0.95(6)	$\frac{21}{2}^+$	$\frac{17}{2}^+$
	230.8	1.8(1)		$\frac{21}{2}^+$	$\frac{19}{2}^-$
1672.6	474.4	5.4(3)	1.0(1)	$\frac{25}{2}^+$	$\frac{21}{2}^+$
2198.8	526.2	<1		$(\frac{29}{2}^+)$	$\frac{25}{2}^+$
[413]5/2, $\alpha=-\frac{1}{2}$					
78.6	78.6 [f]			$\frac{7}{2}^+$	$\frac{5}{2}^+$
300.6	222.0	84(5)	1.02(6)	$\frac{11}{2}^+$	$\frac{7}{2}^+$
	121.6	17(1)		$\frac{11}{2}^+$	$\frac{9}{2}^+$
604.2	303.6	53(3)	1.01(6)	$\frac{15}{2}^+$	$\frac{11}{2}^+$
	161.1	5.7(4)		$\frac{15}{2}^+$	$\frac{13}{2}^+$
	117.5	5.1(4)		$\frac{15}{2}^+$	$\frac{13}{2}^-$
982.5	378.3	27(1)	1.02(5)	$\frac{19}{2}^+$	$\frac{15}{2}^+$
	197.0	2.5(1)		$\frac{19}{2}^+$	$\frac{17}{2}^+$
	181.7	2.3(1)		$\frac{19}{2}^+$	$(\frac{17}{2}^-)$
1427.1	444.6	8.0(4)	1.04(8)	$\frac{23}{2}^+$	$\frac{19}{2}^+$
1929.1	502.0	2.1(1)		$(\frac{27}{2}^+)$	$\frac{23}{2}^+$
[532]5/2, $\alpha=+\frac{1}{2}$					
254.6	85.8	10.3(8)		$\frac{9}{2}^-$	$\frac{7}{2}^-$
	176.0	97(6)	0.76(7) [g]	$\frac{9}{2}^-$	$\frac{7}{2}^+$
487.0	232.4	9.8(5)		$\frac{13}{2}^-$	$\frac{9}{2}^-$
	129.9	19(1)		$\frac{13}{2}^-$	$\frac{11}{2}^-$
	186.5	28(1)	0.65(6) [g]	$\frac{13}{2}^-$	$\frac{11}{2}^+$
801.1	314.1	14.0(7)		$(\frac{17}{2}^-)$	$\frac{13}{2}^-$
	177.1	16.4(8)		$(\frac{17}{2}^-)$	$\frac{15}{2}^-$
	196.8	9.1(5)		$(\frac{17}{2}^-)$	$\frac{15}{2}^+$
1190.6	389.5	9.0(6)		$(\frac{21}{2}^-)$	$(\frac{17}{2}^-)$
	223.2	7.4(4)		$(\frac{21}{2}^-)$	$\frac{19}{2}^-$
	208.2	2.1(2)		$(\frac{21}{2}^-)$	$\frac{19}{2}^+$
(1648.5)	(457.9)	2.0(2)		$(\frac{25}{2}^-)$	$(\frac{21}{2}^-)$
[532]5/2, $\alpha=-\frac{1}{2}$					
169.0	169.0	≈ 15		$\frac{7}{2}^-$	$\frac{5}{2}^+$
357.4	188.4	3.2(2)		$\frac{11}{2}^-$	$\frac{7}{2}^-$
	102.7	12.9(7)		$\frac{11}{2}^-$	$\frac{9}{2}^-$

TABLE II. (*Continued*).

E_x (keV) [a]	E_γ (keV) [b]	I_γ^{rel} [c]	DCO ratio [d]	I_i^π [e]	I_f^π [e]
	178.1	43(2)	0.82(7) [g]	$\frac{11}{2}^-$	$\frac{9}{2}^+$
624.3	266.9	17.8(9)	1.0(1)	$\frac{15}{2}^-$	$\frac{11}{2}^-$
	137.1	19(1)		$\frac{15}{2}^-$	$\frac{13}{2}^-$
	181.3	18(1)	0.62(6) [g]	$\frac{15}{2}^-$	$\frac{13}{2}^+$
967.2	342.9	15.8(8)	1.02(8)	$\frac{19}{2}^-$	$\frac{15}{2}^-$
	165.9	9.0(5)		$\frac{19}{2}^-$	$(\frac{17}{2}^-)$
	181.6	2.9(3)		$\frac{19}{2}^-$	$\frac{17}{2}^+$
1380.2	413.0	6.3(4)	0.97(8)	$\frac{23}{2}^-$	$\frac{19}{2}^-$
	189.4	2.3(3)		$\frac{23}{2}^-$	$(\frac{21}{2}^-)$
	182.1	<1		$\frac{23}{2}^-$	$\frac{21}{2}^+$
[411]3/2, $\alpha=+\frac{1}{2}$					
307.4	61.6 [f]			$\frac{5}{2}^+$	$\frac{3}{2}^+$
500.5	193.1	2.8(4)		$\frac{9}{2}^+$	$\frac{5}{2}^+$
	109.4	8.1(7)		$\frac{9}{2}^+$	$\frac{7}{2}^+$
	331.6	2.7(2)		$\frac{9}{2}^+$	$\frac{7}{2}^-$
781.8	281.3	5.5(4)		$\frac{13}{2}^+$	$\frac{9}{2}^+$
	154.9	5.2(4)		$\frac{13}{2}^+$	$\frac{11}{2}^+$
	424.6	8.0(5)		$\frac{13}{2}^+$	$\frac{11}{2}^-$
1140.2	358.4	4.8(3)		$(\frac{17}{2}^+)$	$\frac{13}{2}^+$
	195.9	3.1(2)		$(\frac{17}{2}^+)$	$(\frac{15}{2}^+)$
	516.0	3.5(3)		$(\frac{17}{2}^+)$	$\frac{15}{2}^-$
1567.6	427.4	2.2(2)		$(\frac{21}{2}^+)$	$(\frac{17}{2}^+)$
[411]3/2, $\alpha=+\frac{1}{2}$					
245.7	245.7	≈ 10		$\frac{3}{2}^+$	$\frac{5}{2}^+$
391.1	145.4	1.0(2)		$\frac{7}{2}^+$	$\frac{3}{2}^+$
	84.1 [f]			$\frac{7}{2}^+$	$\frac{5}{2}^+$
	287.1	3.6(4)		$\frac{7}{2}^+$	$\frac{5}{2}^-$
626.8	235.7	4.2(4)		$\frac{11}{2}^+$	$\frac{7}{2}^+$
	126.2	4.5(4)		$\frac{11}{2}^+$	$\frac{9}{2}^+$
	372.1	8.0(5)		$\frac{11}{2}^+$	$\frac{9}{2}^-$
943.9	317.1	5.4(5)		$(\frac{15}{2}^+)$	$\frac{11}{2}^+$
	161.9	2.6(3)		$(\frac{15}{2}^+)$	$\frac{13}{2}^+$
	457.1	3.0(3)		$(\frac{15}{2}^+)$	$\frac{13}{2}^-$
1332.5	388.6	3.5(3)		$(\frac{19}{2}^+)$	$(\frac{15}{2}^+)$
	532.7	3.1(3)		$(\frac{19}{2}^+)$	$(\frac{17}{2}^-)$
(1785.0)	(452.5)	1.9(4)		$(\frac{23}{2}^+)$	$(\frac{19}{2}^+)$

[a]Level energies; bandhead excitation energies have been taken from previous work [22].
[b]Energies determined from the ^{154}Sm(^{7}Li,4n). Accurate to 0.2 keV for most transitions. For weak or contaminated transitions, accurate to 0.5 keV.
[c]Relative γ-ray intensities [$I_\gamma(179.2)\equiv 100$] measured from the ^{154}Sm(^{7}Li,4n) reaction.
[d]DCO ratios were determined by summing spectra in coincidence with one or more stretched $E2$ transitions as gates.
[e]Spin and parity assignments are based on the previous work [22] and on the DCO ratio determining the multipolarity of any new transition.
[f]Transition was not observed in this work, but was seen in previous publication [22].
[g]DCO value has been contaminated by an unresolvable doublet of different multipolarity.

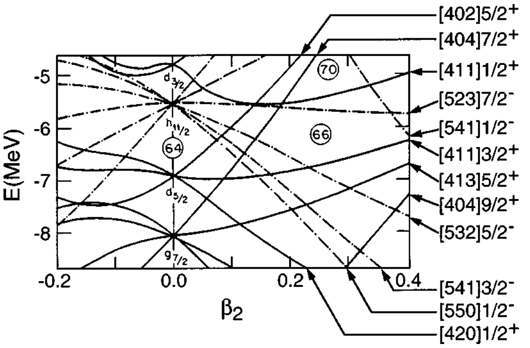

FIG. 3. Single-particle energy diagram [30] for protons in the rare-earth region using a Woods-Saxon potential. Positive (negative) states are shown by solid (dashed) lines. The asymptotic Nilsson quantum numbers $[N,n_z,\Lambda]K^\pi$ are given.

spin assignment. The band overlaps the positive-parity [413]5/2 band in energy above spin $I=\frac{27}{2}$ [Fig. 2(a)] and yet no observed interaction occurs between the bands, so it seems most likely that band 1 has negative parity. By inspecting Fig. 3, one discovers that the nearest negative-parity orbitals to the Fermi surface are the [550]1/2, [541]3/2, and [523]7/2 orbitals. Considering that band 1 is decoupled and the $\alpha=-\frac{1}{2}$ signature is strongly favored, it seems the most likely orbital assignment would be a mixture of the $K^\pi=\frac{1}{2}^-$ and $\frac{3}{2}^-$ orbitals. With the $I=(\frac{11}{2})$ state at an energy of 1047.1 keV, the assignment is in good agreement with Ref. [30], which predicts that the bandhead for the [541]3/2 is near 1 MeV. Further arguments for the suggested assignment of band 1 are given in Sec. III.

5. Band 2

This extremely weak band was not populated to particularly high spin (see Fig. 1); however, we were able to establish the band tentatively up to $I=(\frac{17}{2})$. As seen in Table I, the in-band transitions were all below 1% of the strongest transition in ^{157}Tb. Also, due to the weakness of the band, DCO ratios could not be extracted so the spins are based on the work of Ref. [19]. In Ref. [19], the band was observed up to spin $I=\frac{11}{2}$ and was associated with the negative-parity [523]7/2 proton orbital originating from the $h_{11/2}$ subshell. It has been well established that the $K\leqslant\frac{9}{2}$ members of the $h_{11/2}$ subshell in this region have large signature splitting [1,2]. However, there is no evidence of splitting in band 2 as can be seen in Fig. 2(a). Therefore, negative parity is questioned and we suggest that band 2 originates from some other strongly coupled orbital. Once again by inspecting Fig. 3, two positive-parity orbitals in the region appear to be possible candidates, the [404]7/2 and the [402]5/2. We suggest that band 2 is based on the [404]7/2 orbital simply because it is closer in energy to the Fermi surface. This reassignment is further supported by its alignment properties which are discussed in Sec. III.

B. Level scheme of ^{155}Eu

Previous level schemes for ^{155}Eu can be found in Refs. [21,22]. Reference [21] identified three rotational structures based on the [413]5/2, [532]5/2, and [411]3/2 proton orbitals

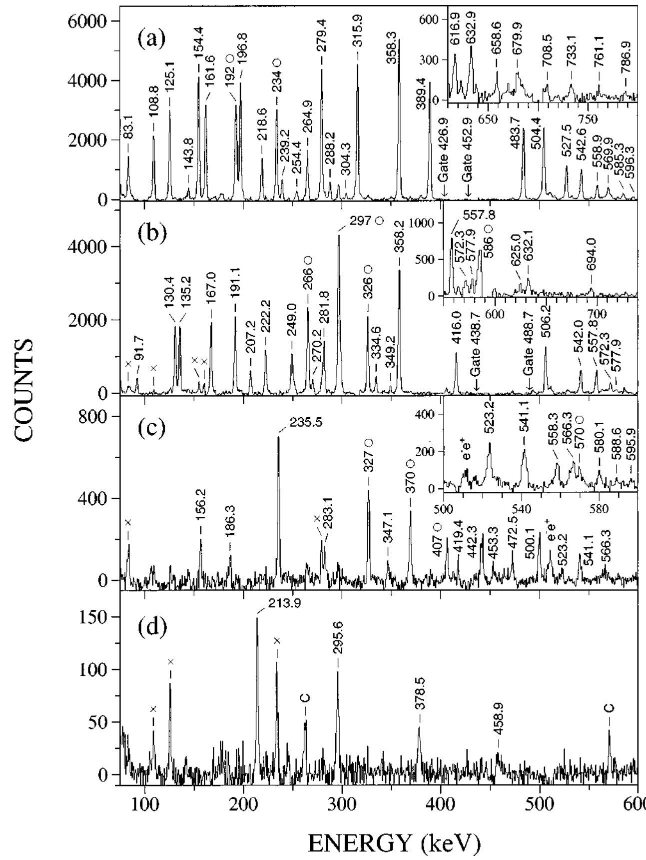

FIG. 4. (a) Spectrum of the [411]3/2 band from summing spectra in coincidence with the 426.9 and 452.9 keV γ rays from the ^{7}Li experiment. The high-energy insert was produced by summing many transitions from the ^{11}B experiment. (b) Spectrum of the [532]5/2 band resulting from transitions in coincidence with the 438.7 and 488.7 keV γ rays in the ^{7}Li experiment. Once again, the high-energy insert was produced by summing many transitions from the ^{11}B experiment. (c) Spectrum of the [413]5/2 band in coincidence with the 369.3, 283.1, and 327.6 keV transitions in the ^{7}Li experiment. A summed spectrum from the ^{11}B experiment is again displayed as an insert. (d) Spectrum of band 1 in coincidence with the 669.6 keV γ ray from the ^{7}Li data. C labels contaminant peaks. In panels (a), (b), and (c), ○ denotes that the transition is at least a doublet and therefore an exact energy cannot be labeled. In panels (b), (c), and (d) transitions in the [411]3/2 band are labeled with an ×.

up to $(\frac{17}{2}^+)$, $(\frac{17}{2}^-)$, and $(\frac{13}{2}^+)$, respectively. Our experiment has extended these bands up to $(\frac{29}{2}^+)$, $(\frac{25}{2}^-)$, and $(\frac{23}{2}^+)$, respectively (Fig. 5), with over 40 new transitions observed. A number of states at high excitation energy reported in Ref. [22] were also seen; however, since no new information was obtained in this work and these states are at low spin ($I<4$), discussion of these levels has been omitted.

1. The [413]5/2 band

Figure 6(a) is a summed spectrum in coincidence with the 303.6 and 342.3 keV transitions in the band. One can observe that the [413]5/2 band feeds the [532]5/2 band through many $\Delta I=1$ transitions (see Fig. 5). This linking of opposite-parity bands by stretched dipoles is similar to that found in lighter nuclei within the lanthanide region and the

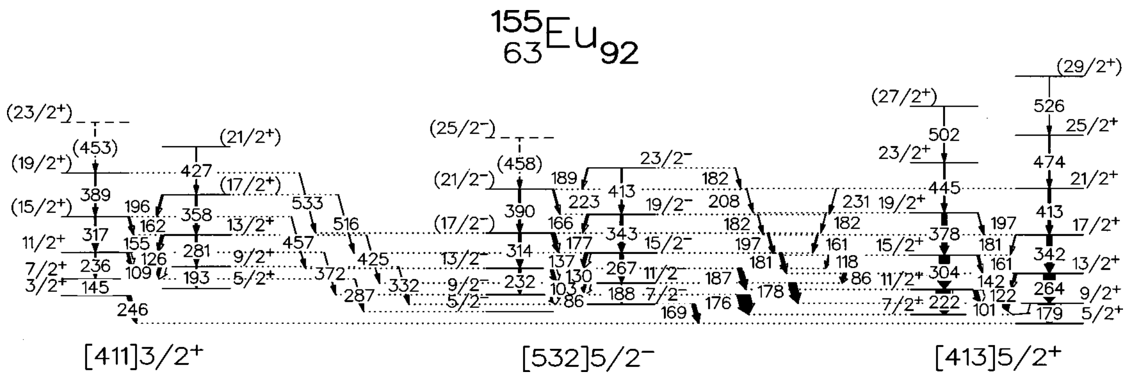

FIG. 5. Level scheme for ^{155}Eu. Tentative transitions and levels are denoted by dashed lines. Spin and parity assignments have been placed within parentheses if reliable DCO measurements were not attainable.

heavier actinide region [33]. By referring to Table II, one may also note the near degeneracy of the states in the [413]5/2 band with the states of equal spin in the [532]5/2 band. Such strongly linked, opposite-parity bands with nearly degenerate levels have been denoted as ''parity-doublet'' bands. The observance of these parity-doublet bands has been associated with octupole correlations, see Ref. [33], and the references therein, which will be discussed in Sec. IV B.

2. The [532]5/2 band

Transitions in coincidence with the 176.0 keV transition, which connects the $\frac{9}{2}^-$ state in the [532]5/2 band to the $\frac{7}{2}^+$ state in the [413]5/2 band, are shown in Fig. 6(b). This negative-parity band also strongly feeds the positive-parity [413]5/2 band through nine $\Delta I = 1$ transitions. It should be noted that the stretched $E2$ transition between the $\frac{9}{2}^- \rightarrow \frac{5}{2}^-$ states was not observed. This 150.2 keV γ ray was not observed in Ref. [21], but weakly ($\approx 1\%$) seen in Ref. [22].

3. The [411]3/2 band

The [411]3/2 band can best be seen by the transitions in coincidence with the $\frac{3}{2}^+ \rightarrow \frac{5}{2}^+$ 245.7 keV transition [Fig. 6(c)]. Efforts to observe the band to even higher spin were greatly impeded by the fact that the entire band is virtually identical (within 2 keV) to the [411]3/2 band in ^{157}Tb. This band in ^{155}Eu is also coupled to the [532]5/2 band by seven $E1$ transitions. Measurement of the $B(E1)/B(E2)$ ratios has allowed the calculation of the $B(E1)$ transition strengths for these $E1$'s as well as those found connecting the [413]5/2 and [532]5/2 bands. Discussion of these properties and of the similarity in the γ-ray energies of various bands follows below.

III. ALIGNMENTS AND BAND CROSSINGS IN ^{157}Tb

The alignment [34] of the bands in ^{157}Tb has been plotted versus rotational frequency in Fig. 7(a) and 7(b). The positive-parity bands are displayed in Fig. 7(a) while the negative-parity bands are shown in Fig. 7(b) for clarity. The Harris parametrization [35] was employed with $\mathcal{J}_0 = 34.3$ $\hbar^2$/MeV and $\mathcal{J}_1 = 45.0$ $\hbar^4$/MeV^3 to subtract a reference term representing the angular momentum contributed by the collective core (^{156}Gd [25]).

The [411]3/2 band undergoes a smooth upbend at $\hbar\omega_c \approx 0.28$ MeV which we attribute to the rotational alignment of two $i_{13/2}$ neutrons (also known as the AB band crossing). The similarity of this crossing frequency ($\hbar\omega_c$) and the observed alignment gain of $\Delta i \approx 9.7$ $\hbar$ to other AB band crossings in neighboring nuclei [34] led to this assignment. The slope of the alignment for the [411]3/2 band is slightly less than the other coupled bands for the AB crossing. This is indicative that a larger interaction strength is involved with the [411]3/2 band than in the [532]5/2 and [413]5/2 bands. Cranked shell model calculations suggest that interaction strengths increase with increasing deformation [34]. Thus a slightly higher deformation may be associated with the [411]3/2 orbital compared to the other bands in ^{157}Tb.

The alignment of the [413]5/2 band is nearly identical to that of the [411]3/2 band over a frequency range of $\hbar\omega \approx 0.05$ to 0.20 MeV. Observing the single-particle diagram in Fig. 3, one can notice that pairs of levels originating from neighboring oscillator shells ($d_{5/2}$ and $g_{7/2}$) are nearly parallel as the quadrupole deformation increases. This creates a large amount of mixing between these levels which results in the large number and strength of transitions connecting the [413]5/2 band to the [411]3/2 band (see Fig. 1). Due to this strong coupling, it may be more appropriate to describe the bands as being pseudospin doublets [36]. In the pseudospin scheme both bands have identical Nilsson values $[\tilde{N}, \tilde{n}_z, \tilde{\Lambda}]$, but differ in $\tilde{\Omega}$ ($\tilde{\Omega} = \tilde{\Lambda} \pm \frac{1}{2}$). It is not surprising then to observe the similar alignment profile at low frequency ($\hbar\omega < 0.20$ MeV) between these bands, which come from the same pseudospin orbital. However, a break in the similarity is found at the alignment of the $i_{13/2}$ neutrons at $\hbar\omega_c \approx 0.28$ MeV. This is likely due to the suggested small difference in deformation between the bands.

Band 2 was originally assigned as the [523]7/2 band in Ref. [19]. However, assuming that the spin assignment of the lowest state is correct, the alignment of the band is contradictory to this assignment. Since the [523]7/2 is a high-j, midshell orbital, some initial alignment would be expected. Instead we observe roughly zero initial alignment which, along with the lack of signature splitting discussed in Sec. II A 5, leads us to suggest that the band may be better associated with the [404]7/2 orbital.

The [532]5/2 band has an initial alignment of $i \approx 1.8\hbar$ and has a gain in alignment at $\hbar\omega_c \approx 0.29$ MeV. The $\alpha = -\frac{1}{2}$

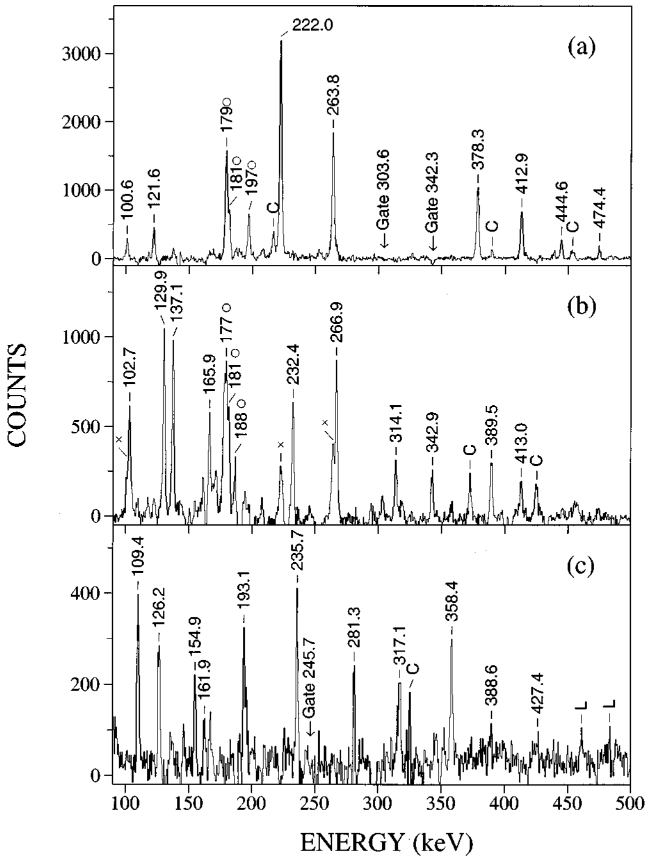

FIG. 6. (a) Spectrum of the [413]5/2 band in coincidence with the 303.6 and 342.3 keV transitions. C labels contaminant peaks. (b) Spectrum of transitions in coincidence with the 176.0 keV γ ray which displays the [532]5/2 band. Transitions in the [413]5/2 band are labeled with an $\times$. (c) Spectrum of the [411]3/2 band in coincidence with the 245.7 keV transition. Peaks labeled with an L are links to higher lying band heads which are mentioned in Sec. II B. In panels (a) and (b), a $\bigcirc$ denotes that the transition is at least a doublet and therefore an exact energy cannot be labeled.

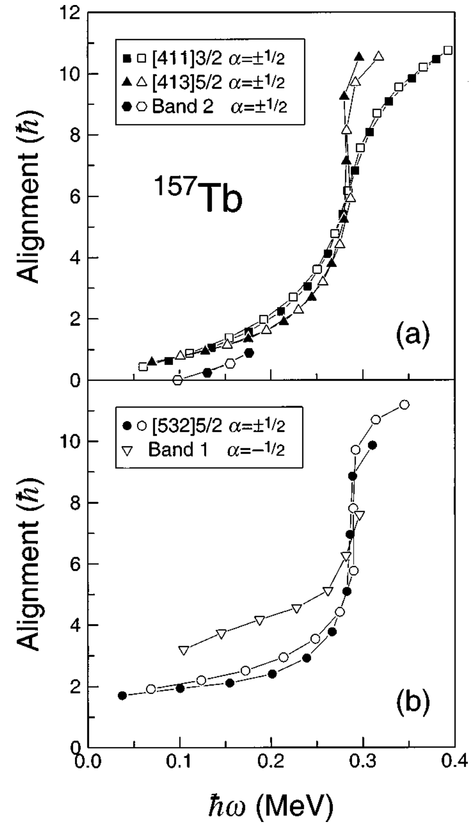

FIG. 7. (a) Alignment plot for the [411]3/2, [413]5/2, and band 2 from ^{157}Tb. (b) Alignment plot for the [532]5/2 and band 1 from ^{157}Tb. The Harris parameters $\mathcal{J}_0=34.3\ \hbar^2/\mathrm{MeV}$ and $\mathcal{J}_1=45\ \hbar^4/\mathrm{MeV}^3$ which gave zero alignment for the low frequency part of the ground-state band in ^{156}Gd were used.

signature has gained $\approx 9.4\hbar$ in alignment and it appears that the $\alpha=+\frac{1}{2}$ signature follows this trend. The alignment of the lowest energy pair of $i_{13/2}$ neutrons is interpreted as being responsible for this gain. The systematics of the *AB* band crossing frequencies for neighboring odd-*Z*, odd-*A* nuclei involving an $h_{11/2}$ proton are discussed below.

Band 1 is too low in energy and spin to be considered as a three-quasiparticle band. The alignment properties of band 1 help in determining its configuration assignment. There are limited choices for possible decoupled bands in this region (see Fig. 3). The [411]1/2 orbital is available, however, the initial alignment of $i\approx 3.2\hbar$ is too high to be a realistic choice. The alignment of band 1 is quite similar to that of the yrast band in ^{153}Tb [18,37,38], which is a mixture of low-*K* $h_{11/2}$ orbitals. This evidence along with the information in Sec. II A 4 has led to the suggested assignment of band 1 as a mixture of the [550]1/2 and [541]3/2 orbitals.

The *AB* band crossing frequencies for the odd-*Z* Tb, Ho, Tm, and Lu nuclei have been plotted in Fig. 8 as a function of neutron number. Bands based on $\pi h_{11/2}$ orbitals are observed in each of the nuclei; therefore, these bands were used to obtain $\hbar\omega_c$. The solid and open symbols represent the crossing frequencies for the $\alpha=+\frac{1}{2}$ and $\alpha=-\frac{1}{2}$ signatures, respectively. Several trends can be observed in Fig. 8.

(1) The $\alpha=-\frac{1}{2}$ signature has a delayed crossing frequency with respect to the $\alpha=+\frac{1}{2}$ signature. However, the difference decreases as the neutron number increases.

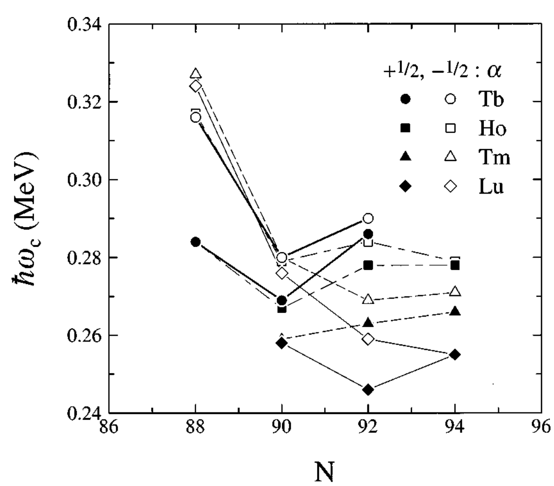

FIG. 8. Systematics of the *AB* band crossing frequency ($\hbar\omega_c$) versus neutron number for the Tb ($Z=65$), Ho ($Z=67$), Tm ($Z=69$), and Lu ($Z=71$) isotopes. The $\alpha=+\frac{1}{2}$ and $\alpha=-\frac{1}{2}$ signatures of the $\pi h_{11/2}$ orbitals are represented by solid and open symbols, respectively.

(2) The crossing frequency is greater in the $N=88$ nuclei than in the $N=90$, 92, and 94 nuclei.

(3) In the $N=92$ and 94 isotones, the crossing frequency systematically increases as Z decreases.

The first trend (1) can be explained by the fact that the $\alpha=-\frac{1}{2}$ signature is energetically favored. Therefore, it takes more rotational energy for the favored signature to reach the interaction region of the three-quasiparticle band (which does not strongly favor either signature initially). As these odd-Z nuclei increase in N, the energy gap between the two signatures decreases. Thereby, the crossing frequencies of the signatures become assimilated.

The last two trends are in good agreement with the observed band crossing systematics in the light rare-earth even-even nuclei. The even-even systematics were investigated in Ref. [39] and we will give a brief summary of their conclusions here. The trends may be understood by the deformation changes with proton and neutron number and the location of the neutron Fermi surface with respect to the lowest pair of down sloping $i_{13/2}$ neutron orbitals. Trend (2) is a result of the $N=88$ nuclei's neutron Fermi surface being further away from the $i_{13/2}$ orbitals than the $N\geqslant 90$ nuclei in the region. This is due to the fewer number of neutrons and the lower deformation of the $N=88$ nuclei. Therefore, a greater rotational energy is necessary for the bands in $N=88$ nuclei to undergo the AB crossing. The third trend (3) can be explained by the fact that the deformation in the isotonic chain increases as Z decreases. For the $N=92$ and 94 nuclei, the neutron Fermi surface is located above the lowest pair of $i_{13/2}$ orbitals. The highest Z (Lu), therefore, has its Fermi surface located nearest these $i_{13/2}$ orbitals and so has the lowest crossing frequency. An inversion of this trend occurs in the $N=88$ nuclei since the Fermi surfaces are below the $i_{13/2}$ orbitals. The $N=88$ nuclei with the highest deformation (Tb/Ho) will be closest in energy to the $i_{13/2}$ orbitals and therefore have the lowest AB crossing frequency.

IV. ELECTROMAGNETIC TRANSITION PROBABILITIES IN ^{155}Eu AND ^{157}Tb

A. $B(M1)/B(E2)$ ratios

Experimental $B(M1)/B(E2)$ values were extracted from the ^{7}Li data using the observed γ-ray energies and branching ratios $[\lambda=I_\gamma(I\rightarrow I-2)/I_\gamma(I\rightarrow I-1)]$ according to the standard formula

$$\frac{B(M1:I\rightarrow I-1)}{B(E2:I\rightarrow I-2)}=0.693\frac{E_\gamma^5(I\rightarrow I-2)}{E_\gamma^3(I\rightarrow I-1)}\times\frac{1}{\lambda(1+\delta^2)}\left(\frac{\mu_N}{e\ \mathrm{b}}\right)^2,$$

where E_γ is in MeV. Rotational model calculations [40] were performed to determine the magnitude of the mixing ratios δ for the $\Delta I=1$ transitions using the measured branching ratios. The results were that the mixing ratios were small ($\delta\leqslant 0.2$) for the [411]3/2 and [532]5/2 in-band $\Delta I=1$ transitions in both nuclei but quite significant for the [413]5/2 in-band $\Delta I=1$ transitions ($\delta\approx 0.6$ and 0.5 for ^{155}Eu and ^{157}Tb, respectively). These mixing ratios were included in the determination of the experimental $B(M1)/B(E2)$ values and the results are shown in Figs. 9(a) and 9(b).

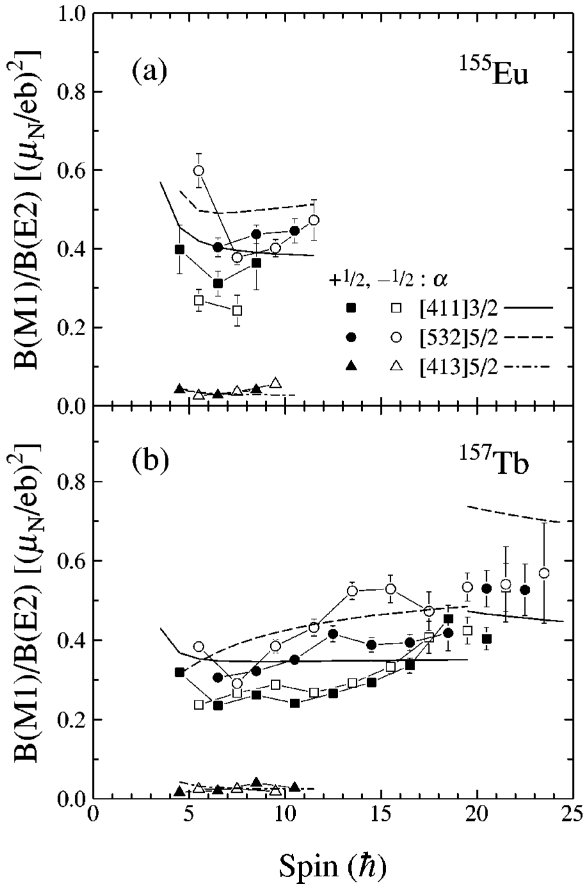

FIG. 9. Experimental and theoretical plots of the $B(M1)/B(E2)$ ratios for (a) ^{155}Eu and (b) ^{157}Tb.

Theoretical calculations have been made using the geometrical model discussed by Dönau [41] and Frauendorf [42]. Quadrupole moments of $Q_0=6.7$ and 6.8 e b were used for ^{155}Eu and ^{157}Tb, respectively. These values were derived by averaging the measured quadrupole moments of the 2^+ states in the nearest even-even nuclei [43]. The other parameters which were utilized in the calculations are displayed in Table III. The value of g_R was taken as $0.7(Z/A)$ and the gyromagnetic ratios (g_K) were obtained from a Woods-Saxon potential [44,45] calculation. The alignments were determined from the low rotational frequency, $\hbar\omega=0.1$ MeV, portion of Fig. 7. Calculations for the three-quasiparticle configurations after the alignment of the $i_{13/2}$ neutrons were also performed for the [411]3/2 and [532]5/2 bands in ^{157}Tb. The parameters used to represent the neutrons are denoted with a (ν) in Table III.

The results of these calculations are displayed along with the experimental results in Fig. 9. There appears to be a general agreement between theory and experiment for all the bands in both nuclei. The theoretical predictions for the ratios of the [411]3/2 bands are somewhat larger than what was experimentally observed. This may well be a result of the mixing of the [411]3/2 and the [413]5/2 bands from the pseudospin symmetry discussed in Sec. III. One can also observe the signature dependence of the experimentally extracted values of the [532]5/2 band in ^{157}Tb. This adds valuable data to the systematic study of the signature effects of the bands based on the $\pi h_{11/2}$ orbitals in this region.

TABLE III. Parameters used in the calculation of $B(M1)/B(E2)$ ratios.

Band	g_R	g_K	K ($\hbar$)	i ($\hbar$)	$g_K(\nu)$	$K(\nu)$ ($\hbar$)	$i(\nu)$ ($\hbar$)
				^{155}Eu			
[411]3/2	0.28	1.81	3/2	0.5			
[532]5/2	0.28	1.43	5/2	1.5			
[413]5/2	0.28	0.53	5/2	0.8			
				^{157}Tb			
[411]3/2	0.29	1.81	3/2	0.8	−0.20	0	9.7
[532]5/2	0.29	1.43	5/2	2.0	−0.20	0	9.4
[413]5/2	0.29	0.53	5/2	0.7			

In the ^{7}Li experiment, reliable dipole transitions were observed up to spin $I=\frac{37}{2}$ in ^{157}Tb. However, the ^{11}B experiment disclosed a few more intraband transitions and the resulting $B(M1)/B(E2)$ ratios are displayed in Fig. 9(b) without line connections. The $B(M1)/B(E2)$ ratios begin to rise in the [411]3/2 band above spin $I=\frac{33}{2}$ to values of ≈ 0.4 $(\mu_N/e\ \mathrm{b})^2$. This may be attributed to the neutron alignment as can be seen by the theoretical prediction that ratios of ≈ 0.45 $(\mu_N/e\ \mathrm{b})^2$ should be reached after the alignment. There is a steady rise in the $B(M1)/B(E2)$ values throughout the spin region for the [532]5/2 band. However, the calculations suggest that the ratios should rise to ≈ 0.7 $(\mu_N/e\ \mathrm{b})^2$ once the neutrons become fully aligned. Unfortunately, we were not able to establish the band up all the way through the band crossing region to test this prediction.

B. $B(E1)/B(E2)$ ratios

Experimentally determined $B(E1)/B(E2)$ ratios were extracted using the γ-ray energies and branching ratios (λ) using the formula

$$\frac{B(E1:I\to I-1)}{B(E2:I\to I-2)}=0.767\frac{1}{\lambda}\frac{E_\gamma^5(I\to I-2)}{E_\gamma^3(I\to I-1)}(10^{-6}\ \ \mathrm{fm}^{-2}),$$

where E_γ is in MeV. The results for ^{155}Eu and ^{157}Tb are displayed in Table IV along with the calculated $B(E2)$ values, and the deduced $B(E1)$ strengths. The rates between the $K^\pi=\frac{5}{2}^+$ and $\frac{5}{2}^-$ bands in ^{155}Eu are $\approx 1\times 10^{-3}$ Weisskopf units (1 W.u. $\approx 1.87\ e^2\ \mathrm{fm}^2$ for $A\approx 155$), while in ^{157}Tb the $B(E1)$ strengths between the same bands are $\approx 2\times 10^{-4}$ Weisskopf units. We can determine an average electric dipole moment $|D_0|$ for these nuclei using the equation [40]

$$B(E1)=\frac{3}{4\pi}D_0^2\langle IK10|(I-1)K\rangle^2.$$

After averaging the $B(E1)$ values and using an average spin of $I=\frac{17}{2}$ for both nuclei, electric dipole moments of $|D_0|$ = 0.14(3) and 0.06(1) e fm were found for ^{155}Eu and ^{157}Tb, respectively. These values are very similar to the electric dipole moments in the Ba-Sm region where octupole correlations are believed to be quite prevalent [33]. The transitions connecting the $K^\pi=\frac{5}{2}^-$ and $\frac{3}{2}^+$ bands have smaller $B(E1)$ strengths compared with the $\Delta K=0$ transitions, but they are still considerably large ($\approx 1\times 10^{-4}$ and $\approx 5\times 10^{-5}$ W.u. for ^{155}Eu and ^{157}Tb, respectively).

It is well known that low-energy $E1$ transitions are not favored and that $B(E1)$ strengths are typically 10^{-6} W.u. in atomic nuclei. However, small regions of nuclei have been found in the actinide and lanthanide series which have transitions strengths 100 times or more stronger than those found in other nuclei [33]. Much work has been done to explain this phenomenon and the possibility of stable octupole deformation has been suggested as a likely scenario. Theoretical predictions find that nuclei with $Z\approx 58$, $N\approx 88$ are good candidates for octupole deformation [46]. Since ^{155}Eu and ^{157}Tb have $Z=63$ and 65, respectively, and $N=92$, these nuclei are somewhat removed from the predicted areas of stable octupole deformation. However, strong octupole correlations have been invoked in the discussion of phenomena observed in the $N=90$ nuclei ^{151}Pm [10,11] and ^{153}Eu [16,17].

Parity-doublet bands have been predicted to be evidence for octupole shapes as the bands arise from the same asymmetric reflection state [47]. The apparent parity-doublet bands found in the Pm/Eu region have led theorists to investigate these $K^\pi=\frac{5}{2}^\pm$ bands using the quasiparticle phonon nuclear model (QPNM) [47] and the particle-rotor model [48]. The conclusions from both of the studies were that the enhanced $E1$ transition strengths were not from the singly occupied orbitals driving the nuclei to an octupole shape. Instead, both Refs. [47,48] cite the QPNM+particle-rotor calculations in Ref. [49] to explain the large $B(E1)$ strengths. The calculations in Ref. [49] found that large contributions to the $\mathcal{M}(E1)$ matrix elements of odd-A Eu and Tb nuclei come from the enhanced $E1(\Delta K=0)$ transitions in the even-even cores. The lower $B(E1)$ strengths for the $E1(\Delta K=1)$ transitions were also well reproduced with the QPNM+particle-rotor model. The small energy splitting of the states between the $K^\pi=\frac{5}{2}^\pm$ bands was then suggested as an accidental near degeneracy of the two Nilsson orbitals [48]. Our data appear to further support these conclusions as the $B(M1)/B(E2)$ ratios in Fig. 9(a) for the $K^\pi=\frac{5}{2}^\pm$ bands are decisively different. The bands resulting from an asymmetric reflection state would have similar magnetic moments

TABLE IV. The measured $B(E1)/B(E2)$ ratios with the calculated $B(E1)$ and $B(E2)$ transition rates.

I_i^π	E_γ (keV)	$B(E1)/B(E2)$ ($\times 10^{-7}$ fm^{-2})	$B(E2)$ [a] ($\times 10^{4}$ e^2 fm^4)	$B(E1)$ ($\times 10^{-3}$ e^2 fm^2)
		^{155}Eu		
[413]5/2→[532]5/2				
$\frac{13}{2}^+$	85.8	2.2(2)	0.96	2.1(2)
$\frac{15}{2}^+$	117.5	1.2(1)	1.10	1.3(1)
$\frac{17}{2}^+$	160.8	1.9(1)	1.20	2.2(2)
$\frac{19}{2}^+$	181.7	0.8(1)	1.28	1.1(1)
$\frac{21}{2}^+$	230.8	1.1(1)	1.33	1.4(1)
[532]5/2→[413]5/2				
$\frac{11}{2}^-$	178.1	4.2(3)	0.76	3.2(3)
$\frac{13}{2}^-$	186.5	2.3(1)	0.96	2.2(1)
$\frac{15}{2}^-$	181.3	1.8(1)	1.10	2.0(1)
$(\frac{17}{2}^-)$	196.8	2.0(1)	1.20	2.4(2)
$\frac{19}{2}^-$	181.6	1.1(1)	1.28	1.4(2)
$(\frac{21}{2}^-)$	208.2	1.8(2)	1.33	2.4(2)
$\frac{23}{2}^-$	182.1	1.4(4)	1.38	1.9(6)
[411]3/2→[532]5/2				
$\frac{7}{2}^+$	287.1	0.13(4)	0.64	0.08(3)
$\frac{9}{2}^+$	331.6	0.06(1)	0.96	0.06(1)
$\frac{11}{2}^+$	372.1	0.12(1)	1.14	0.14(1)
$\frac{13}{2}^+$	424.6	0.26(2)	1.25	0.33(3)
$(\frac{15}{2}^+)$	457.1	0.14(2)	1.33	0.19(3)
$(\frac{17}{2}^+)$	516.0	0.24(4)	1.38	0.33(6)
$(\frac{19}{2}^+)$	532.7	0.47(8)	1.42	0.7(1)
		^{157}Tb		
[532]5/2→[411]3/2				
$\frac{11}{2}^-$	265.0	0.11(1)	0.78	0.09(1)
$\frac{13}{2}^-$	270.2	0.08(1)	0.99	0.08(1)
$\frac{15}{2}^-$	251.2	0.07(1)	1.14	0.08(1)
$\frac{17}{2}^-$	280.8	0.08(1)	1.24	0.10(1)
[413]5/2→[532]5/2				
$\frac{9}{2}^+$	156.2	0.65(4)	0.46	0.30(2)
$\frac{11}{2}^+$	217.7	0.47(3)	0.78	0.37(3)
$\frac{13}{2}^+$	279.4	0.45(2)	0.99	0.45(3)
$\frac{15}{2}^+$	322.7	0.32(2)	1.14	0.37(3)
$\frac{17}{2}^+$	383.3	0.28(1)	1.24	0.35(2)
$\frac{19}{2}^+$	402.6	0.28(1)	1.32	0.37(2)
$\frac{21}{2}^+$	467.2	0.22(1)	1.37	0.30(2)
$\frac{23}{2}^+$	459.0	0.18(1)	1.42	0.26(2)
$\frac{25}{2}^+$	528.7	0.22(1)	1.45	0.32(3)

[a] $B(E2)$ values calculated using $B(E2) = (5/16\pi) Q_0^2 \langle I_i K_i 20 | I_f K_f \rangle^2$, where $Q_0 = 6.7$ e b and 6.8 e b for ^{155}Eu and ^{157}Tb, respectively.

[47], which would lead to similar $B(M1)/B(E2)$ ratios in the parity-doublet bands. Since this is not the case in the ^{155}Eu parity-doublet bands and that there is a lack of parity-doublet bands in ^{157}Tb, it appears unlikely that these nuclei are octupole deformed. Therefore, our experimental results are in agreement with the conclusions of Refs. [47,48].

V. IDENTICAL [411]3/2 BANDS IN ^{155}Eu AND ^{157}Tb

The discovery of identical superdeformed bands led to great excitement recently which launched a search for identical bands in normal deformed nuclei. Numerous normal deformed bands having strikingly similar moments of inertia were found between even-even neighbors, adjacent even and odd-A nuclei, nearby odd-A nuclei, and even within the same nuclei (see Ref. [50], and references therein). Several identical normal deformed bands have been found between neighboring odd-A nuclei involving the [402]5/2 and [404]7/2 proton orbitals in the $A\approx170$ region [50]. In the present study we observe bands based on the midshell $d_{5/2}$ proton orbital being identical to each other in the nearby odd-A nuclei ^{155}Eu and ^{157}Tb.

By inspecting the level schemes in Figs. 1 and 5, one can quickly observe the near duplication of the [411]3/2 bands between the two nuclei. In fact by referring to Tables I and II, one finds that all 15 transitions in this band from ^{155}Eu are within 2 keV to the γ rays from ^{157}Tb. Using the criteria defined in Ref. [50], we may classify the bands as identical if the fractional change (FC) in the dynamical moment of inertia

$$\mathrm{FC}=\frac{J_A^{(2)}-J_B^{(2)}}{J_A^{(2)}}$$

of the bands is no larger than $\approx 1-2\,\%$. We found the fractional change of the [411]3/2 bands to be FC$\approx$1.0%. This is similar to that established between the [404]7/2 bands in ^{169}Tm [51] and ^{173}Lu [52]. However, the difference between the identical bands in ^{155}Eu and ^{157}Tb and those in ^{169}Tm and ^{173}Lu is that the cores for the $N=92$ nuclei are not identical as the cores are for ^{169}Tm (^{168}Er [53]) and ^{173}Lu (^{172}Yb [54]). In fact, the general explanation for identical bands between nearby odd-A nuclei is that they result from the same spectator particle coupling to two identical even-even nuclei [50]. In Fig. 10(a) we have plotted the energy differences (ΔE_γ) between the stretched $E2$ transitions of the known bands in ^{155}Eu and ^{157}Tb versus the energy of the ^{157}Tb transitions as well as the ΔE_γ of the ground-state bands in ^{154}Sm and ^{156}Gd versus the energy of the ^{156}Gd transitions. While the [411]3/2 bands have $\Delta E_\gamma\approx\pm2$ keV it is quite clear that there is a divergence between the other bands in ^{155}Eu and ^{157}Tb as well as the ground-state bands in the even-even cores of ^{155}Eu and ^{157}Tb.

Therefore, if the core is not the cause of the identical bands, then is it the valence orbital that is responsible? By inspecting Figs. 10(a) and 10(b), we can make a few observations about the [411]3/2 orbital in this region. First, one can see a pattern developing in the other orbitals of ^{155}Eu and ^{157}Tb as well as in the $N=90$ nuclei ^{153}Eu [16] and ^{155}Tb [18–20,55] in Fig. 10(b). The $K^\pi=\frac{5}{2}^\pm$ bands in the Tb nuclei have larger $E2$ transition energies than in the Eu nuclei which give the negative values seen in the figure. This

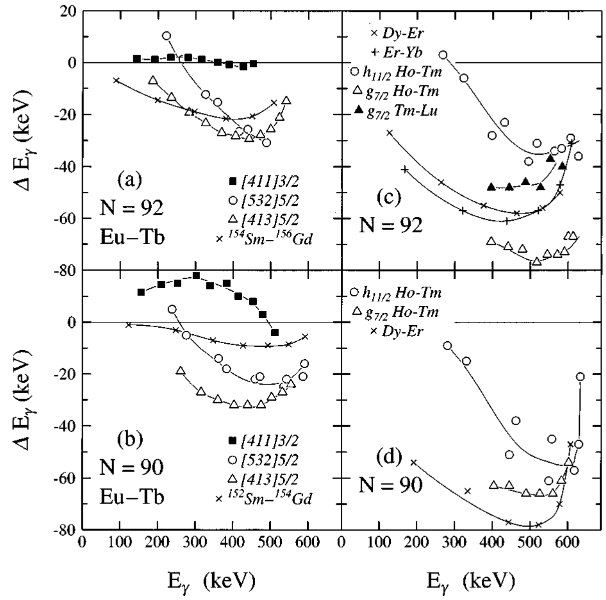

FIG. 10. Energy differences ΔE_γ between similar bands in the (a) $N=92$ and (b) $N=90$ Eu and Tb nuclei. The energy difference between the ground-state bands of the Sm and Gd nuclei have also been included for discussion. Note that $\Delta E_\gamma=E_\gamma(A_a)-E_\gamma(A_b)$ where $A_b>A_a$. The ΔE_γ of bands in neighboring (c) $N=92$ and (d) $N=90$ nuclei are also plotted with their respective cores.

indicates a slight decrease in the moment of inertia in the heavier nuclei. The ΔE_γ for all the orbitals in the neighboring $N=92$ and 90 nuclei is also given in Figs. 10(c) and 10(d). The same pattern as seen in the $K^\pi=\frac{5}{2}^\pm$ bands of the Eu and Tb nuclei is observed in these bands. However, as discussed above, the [411]3/2 orbital in the $N=92$ Eu/Tb nuclei have an energy difference of ≈0 keV and the $N=90$ Eu/Tb nuclei have an energy difference of about $+15$ keV even though the cores for the latter are nearly identical. One can also observe that in both examples the [411]3/2 band lies ≈20 keV above the energy difference of the cores. From these two cases, there appears to be some anomaly concerning this midshell $d_{5/2}$ orbital. Unfortunately, there is no other reliable pair of [411]3/2 bands to compare with the Eu/Tb nuclei in the $N=90$, 92 Ho, Tm, and Lu nuclei.

The observed behavior of the [411]3/2 orbital is consistent with the results of our alignment analysis. It was stated in Sec. III that the [411]3/2 orbital may have a larger deformation than the other bands in ^{157}Tb as suggested from the larger interaction strength observed at the AB crossing. Similar interaction strength results are obtained from the same rotational bands in ^{155}Tb [18]. Therefore, an increase in deformation gives the [411]3/2 band a larger moment of inertia as compared to the other bands and seemingly just enough in ^{157}Tb to make it identical to the [411]3/2 band in ^{155}Eu. Unfortunately, the [411]3/2 bands in ^{153,155}Eu have not been extended into the band crossing region in order to make the same interaction strength comparison possible.

VI. SUMMARY

In summary, we have placed over 100 new transitions in the level scheme of ^{157}Tb. The massive transfer reaction in the ^{7}Li experiment allowed the extension to higher spin of three bands in ^{155}Eu. The first $i_{13/2}$ neutron band crossing systematics for odd-Z rare-earth ($N=88-94$) nuclei were studied and shown to be consistent with those of the even-even nuclei. Extracted $B(M1)/B(E2)$ ratios for both ^{155}Eu and ^{157}Tb compared well with the geometrical model calculations for their given configurations. Unusually large $B(E1)$ transitions strengths were observed in both nuclei and attributed to contributions from the even-even cores rather than stable octupole deformation. Identical [411]3/2 bands were found in the ^{155}Eu and ^{157}Tb nuclei even though their respective cores are not identical. Rotational alignment analysis offered evidence for a slightly larger deformation in the [411]3/2 band of ^{157}Tb compared to the other ^{157}Tb bands helping to give it an identical moment of inertia to that found in the [411]3/2 band of ^{155}Eu.

ACKNOWLEDGMENTS

Special thanks to D. C. Radford and H. Q. Jin for their software support and also to R. Darlington for help with the targets. Helpful discussions and suggestions from L. P. Ekström are gratefully acknowledged. Support for this work was provided by the U.S. Department of Energy, the National Science Foundation, the State of Florida, and the U.K. Engineering and Physical Science Research Council. M.A.R. and J.S. acknowledge the receipt of a NATO Collaborative Research Grant.

[1] I. Hamamoto and H. Sagawa, Phys. Lett. B **201**, 415 (1988).

[2] A. Ikeda and T. Shimano, Phys. Rev. C **42**, 149 (1990).

[3] S. Frauendorf and F. R. May, Phys. Lett. **125B**, 245 (1983).

[4] Y. S. Chen, S. Frauendorf, and L. L. Riedinger, Phys. Lett. B **171**, 7 (1986).

[5] J. Simpson, P. D. Forsyth, D. Howe, B. M. Nyakó, M. A. Riley, J. F. Sharpey-Schafer, J. Bacelar, J. D. Garrett, G. B. Hagemann, B. Herskind, A. Holm, and P. O. Tjǿm, Phys. Rev. Lett. **54**, 1132 (1985).

[6] D. C. Radford, H. R. Andrews, G. C. Ball, D. Horn, D. Ward, F. Banville, S. Flibotte, S. Monaro, S. Pilotte, P. Taras, J. K. Johansson, D. Tucker, J. C. Waddington, M. A. Riley, G. B. Hagemann, and I. Hamamoto, Nucl. Phys. **A545**, 665 (1992).

[7] W. Urban, T. Rząca-Urban, J. L. Durell, Ch. P. Hess, C. J. Pearson, W. R. Phillips, B. J. Varley, W. J. Vermeer, Ch. Vieu, J. S. Dionisio, M. Pautrat, and J. C. Bacelar, Phys. Rev. C **54**, 2264 (1996).

[8] W. Urban, J. L. Durell, W. R. Phillips, B. J. Varley, Ch. P. Hess, M. A. Jones, C. J. Pearson, W. J. Vermeer, Ch. Vieu, J. S. Dionisio, M. Pautrat, and J. C. Bacelar, Nucl. Phys. **A587**, 541 (1995).

[9] M. A. Jones, W. Urban, J. L. Durell, M. Leddy, W. R. Phillips, B. J. Varley, P. J. Dagnall, A. G. Smith, D. M. Thompson, Ch. Vieu, J. S. Dionisio, C. Schuck, and M. Pautrat, Nucl. Phys. **A609**, 201 (1996).

[10] W. Urban, J. C. Bacelar, W. Gast, G. Hebbinghaus, A. Krämer-Flecken, R. M. Lieder, T. Morek, and T. Rząca-Urban, Phys. Lett. B **247**, 238 (1990).

[11] W. J. Vermeer, M. K. Khan, A. S. Mowbray, J. B. Fitzgerald, J. A. Cizewski, B. J. Varley, J. L. Durell, and W. R. Phillips, Phys. Rev. C **42**, R1183 (1990).

[12] W. Urban, J. C. Bacelar, J. R. Jongman, R. F. Noorman, M. J. A. de Voigt, J. Nyberg, G. Sletten, M. Bergström, and H. Ryde, Nucl. Phys. **A578**, 204 (1994).

[13] J. R. Jongman, J. C. S. Bacelar, W. Urban, R. F. Noorman, J. van Pol, Th. Steenbergen, M. J. A. de Voigt, J. Nyberg, G. Sletten, J. Dionisio, and Ch. Vieu, Phys. Rev. C **50**, 3159 (1994).

[14] W. J. Vermeer, W. Urban, M. K. Khan, C. J. Pearson, A. B. Wiseman, B. J. Varley, J. L. Durell, and W. R. Phillips, Nucl. Phys. **A559**, 422 (1993).

[15] J. R. Jongman, W. Urban, J. C. S. Bacelar, J. van Pol, J. Nyberg, G. Sletten, J. S. Dionisio, Ch. Vieu, J. M. Lagrange, and M. Pautrat, Nucl. Phys. **A591**, 244 (1995).

[16] C. J. Pearson, W. R. Phillips, J. L. Durell, B. J. Varley, W. J. Vermeer, W. Urban, and M. K. Khan, Phys. Rev. C **49**, R1239 (1994).

[17] S. Basu, S. Chattopadhyay, J. M. Chatterjee, R. K. Chattopadhyay, S. S. Ghugre, G. Rodrigues, R. P. Singh, S. Murulithar, and R. K. Bhowmik, Phys. Rev. C **56**, 1756 (1997).

[18] D. J. Hartley *et al.* (unpublished).

[19] G. Winter, L. Funke, K.-H. Kaun, P. Kemnitz, and H. Sodan, Nucl. Phys. **A176**, 609 (1971).

[20] J. C. Tippett and D. G. Burke, Can. J. Phys. **50**, 3152 (1972).

[21] R. Katajanheimo, H. Liljavirta, A. Siivola, E. Hammarén, and E. Liukkonen, Z. Phys. A **319**, 91 (1984).

[22] P. T. Prokofjev, V. A. Bondarenko, T. V. Guseva, N. D. Kramer, L. I. Simonova, J. J. Tambergs, K. Schreckenbach, W. F. Davidson, J. A. Pinston, D. D. Warner, P. H. M. Van Assche, and A. M. J. Spits, Nucl. Phys. **A455**, 1 (1986).

[23] S. L. Tabor, M. A. Riley, J. Döring, P. D. Cottle, R. Books, T. Glasmacher, J. W. Holcomb, J. Hutchins, G. D. Johns, T. D. Johnson, T. Petters, O. Tekyi-Mensah, P. C. Womble, L. Wright, and J. X. Saladin, Nucl. Instrum. Methods Phys. Res. B **79**, 821 (1993).

[24] D. R. Zolnowski, H. Yamada, S. E. Cala, A. C. Kahler, and T. T. Sugihara, Phys. Rev. Lett. **41**, 92 (1978).

[25] J. Konijn, F. W. N. de Boer, A. van Poelgeest, W. H. A. Hesselink, M. J. A. de Voigt, H. Verheul, and O. Scholten, Nucl. Phys. **A352**, 191 (1981).

[26] D. C. Radford, Nucl. Instrum. Methods Phys. Res. A **361**, 297 (1995).

[27] R. B. Firestone, *Table of Isotopes*, edited by V. S. Shirley, C. M. Baglin, S. Y. F. Chu, and J. Zipken (Wiley, New York, 1996), Vol. 2.

[28] R. G. Helmer, Nucl. Data Sheets **78**, 219 (1996).

[29] K. S. Krane, R. M. Steffen, and R. M. Wheeler, Nucl. Data Tables **11**, 351 (1973).

[30] W. Nazarewicz, M. A. Riley, and J. D. Garrett, Nucl. Phys. **A512**, 61 (1990).

[31] L. Funke, H. Graber, K.-H. Kaun, H. Sodan, L. Werner, and J. Frána, Nucl. Phys. **84**, 449 (1966).

[32] P. H. Blichert-Toft, E. G. Funk, and J. W. Mihelich, Nucl. Phys. **A100**, 369 (1967).

[33] P. A. Butler and W. Nazarewicz, Rev. Mod. Phys. **68**, 349 (1996).

[34] R. Bengtsson, S. Frauendorf, and F.-R. May, At. Data Nucl. Data Tables **35**, 15 (1986).
[35] S. M. Harris, Phys. Rev. **138**, B509 (1965).
[36] R. D. Ratna Raju, J. P. Draayer, and K. T. Hecht, Nucl. Phys. **A202**, 433 (1973).
[37] G. Winter, J. Döring, L. Funke, P. Kemnitz, E. Will, S. Elfström, S. A. Hjorth, A. Johnson, and Th. Lindblad, Nucl. Phys. **A299**, 285 (1978).
[38] M. D. Devous, Sr. and T. T. Sugihara, Z. Phys. A **288**, 79 (1978).
[39] J. Simpson, M. A. Riley, A. Alderson, M. A. Bentley, A. M. Bruce, D. M. Cullen, P. Fallon, F. Hanna, and L. Walker, J. Phys. G **17**, 511 (1991).
[40] A. Bohr and B. R. Mottelson, *Nuclear Structure* (Benjamin, New York, 1975), Vol. 2.
[41] F. Dönau, Nucl. Phys. **A471**, 469 (1987).
[42] S. Frauendorf, Phys. Lett. **100B**, 219 (1981).
[43] S. Raman, C. H. Malarkey, W. T. Milner, C. W. Nestor, Jr., and P. H. Stelson, At. Data Nucl. Data Tables **36**, 1 (1987).
[44] S. Ćwiok, J. Dudek, W. Nazarewicz, J. Skalski, and T. Werner, Comput. Phys. Commun. **46**, 379 (1987).
[45] J. Dudek, A. Majhofer, J. Skalski, T. Werner, S. Ćwiok, and W. Nazarewicz, J. Phys. G **5**, 1359 (1979).
[46] W. Nazarewicz and S. L. Tabor, Phys. Rev. C **45**, 2226 (1992).
[47] D. Nosek, R. K. Sheline, P. C. Sood, and J. Kvasil, Z. Phys. A **344**, 277 (1993).
[48] A.V. Afanasjev and I. Ragnarsson, Phys. Rev. C **51**, 1259 (1995).
[49] B. A. Alikov, Kh. N. Badalov, V. O. Nesterenko, A. V. Sushkov, and J. Wawryszczuk, Z. Phys. A **331**, 265 (1988).
[50] C. Baktash, B. Haas, and W. Nazarewicz, Annu. Rev. Nucl. Part. Sci. **45**, 485 (1995).
[51] D. Barnéoud, C. Foin, S. André, H. Abou-Leila, and S. A. Hjorth, Nucl. Phys. **A230**, 445 (1974).
[52] P. Kemnitz, L. Funke, K.-H. Kaun, H. Sodan, G. Winter, and M. I. Baznat, Nucl. Phys. **A209**, 271 (1973).
[53] B. Kotliński, D. Cline, A. Bäcklin, K. G. Helmer, A. E. Kavka, W. J. Kernan, E. G. Vogt, C. Y. Wu, R. M. Diamond, A. O. Macchiavelli, and M. A. Deleplanque, Nucl. Phys. **A517**, 365 (1990).
[54] P. M. Walker, S. R. Faber, W. H. Bentley, R. M. Ronningen, and R. B. Firestone, Nucl. Phys. **A343**, 45 (1980).
[55] M. A. Riley, D. J. Hartley, J. Simpson, J. F. Sharpey-Schafer, D. E. Archer, T. B. Brown, J. Döring, P. Fallon, C. A. Kalfas, and S. L. Tabor, Phys. Rev. C **53**, 989 (1996).